JNCS Journal of Nepal Chemical Society July 2025, Vol. 45, No. 2, 84-99
ISSN: 2091-0304 (print)
DOI: https://doi.org/10.3126/jncs.v45i2.83038
RESEARCH ARTICLE

Quantum Chemical Exploration of Carbonofluoridic Acid's Structural, Electronic, and Spectroscopic Properties

Khakendra Basnet[1], Bhijan Neupane[1*]

[1]*Department of Physics, Patan Multiple Campus, Lalitpur, Tribhuvan University, Nepal*

[*]*Corresponding E-mail: bhijanneupane@gmail.com*

(Received: June 10, 2025, revised: June 25, 2025 accepted: July 25, 2025)

Abstract

The structural and electronic properties of the title molecule were investigated using Density Functional Theory (DFT) at the B3LYP/6-311G++(d,p) level in Gaussian G09 W and GaussView. Geometrical optimization was performed to determine the most stable configuration, with total energy computations revealing the minimized energy state. The electronic properties were analyzed through HOMO-LUMO gap calculations, yielding a band gap of 8.68708 eV, indicating high kinetic stability and low reactivity. Global reactivity indices, including electrophilicity, hardness, and electronegativity, were evaluated to ascertain the chemical behavior of the molecule. Molecular Electrostatic Potential (MEP) analysis identified reactive sites, with oxygen atoms showing a negative potential for electrophilic attack, while hydrogen atoms exhibited a positive potential, favoring nucleophilic interactions. Frontier molecular orbitals were further explored using the Total, Partial, and Overlap Density of States (TDOS, PDOS, and OPDOS) to elucidate the charge distribution and orbital contributions. Electron Localization Function (ELF) and Localized Orbital Locator (LOL) analyses revealed the electron density distribution, highlighting regions of strong covalent interactions and localized bonding characteristics. A Reduced Density Gradient (RDG) was employed to visualize non-covalent interactions, indicating van der Waals interactions and steric effects. Fukui functions and dual descriptors were calculated to predict reactive sites and charge-transfer tendencies. Spectroscopic characterization via FT-IR and FT-Raman spectroscopy confirmed the key functional group vibrations. These insights contribute to the understanding of the reactivity and stability of the title molecule and its potential applications in materials science and biochemistry.

Keywords: Vibrational spectra, DFT, Fukui function, ELF & LOL, RDG

Introduction

Carbonofluoridic acid ($CHFO_2$), a specialized fluorine chemical compound, plays a crucial role in the production of advanced materials, as well as in pharmaceutical research. Quantum chemical analysis forms the basis of our research on its behavior as an organic carbonic acid. $CHFO_2$ demonstrates a distinctive chemical behavior that provides essential benefits for synthesizing fluorinated products; however, human contact starting in the prenatal period triggers various health consequences that persist across the human lifespan. In quantum chemistry, quantum mechanics concepts can be used to study the behavior of atoms and molecules [1]. Jones et al. (2016) established a single-step transformation of polycarbonate waste to produce (aryl ether sulfones)s through carbonate salt reactions to establish a sustainable waste-to-use approach [2]. Aggarwal et al. (2021) examined the progress of deoxyfluorination by investigating novel fluorine incorporation reagents for pharmaceutical and biologically active

molecules [3]. The research team of Song et al. (2020) introduced trifluoromethyl trifluoromethanesulfonate ($CF_3SO_2OCF_3$) which serves as a highly efficient fluorinating agent for carboxylic acids to perform deoxyfluorination reactions under mild conditions [4]. Tafrishi et al. (2023) studied the effect of electron bombardment on 2-(trifluoromethyl)acrylic acid (TFMAA) and investigated its use as an extreme ultraviolet lithography (EUVL) resist material component, mainly because of its ability to increase absorption and break molecular bonds for better semiconductor production [5].

Carbonofluoridic acid has not yet been the subject of in-depth theoretical investigation with appropriate theoretical underpinnings. Specifically, density functional theory (DFT)-based quantum chemical analysis techniques were used to thoroughly investigate carbonofluoridic acid. Studying carbonofluoridic acid is important because it can lead to a better understanding of the fields of medicine, materials science, reaction engineering, fluorine chemistry, and its applications.

Methodology

An important first step in this study was to optimize the shape of the molecule. The quantum mechanical modeling method known as density functional theory (DFT) was used to perform this optimization [6]. Popular and widely used Gaussian G09W and GaussView software for computational chemistry have been used for this purpose [7,8]. The advantages of DFT were combined in this study's computational analysis using the B3LYP hybrid functional. The analysis used the 6-311++G(d,p) basis set because it integrates the computational speed with high-precision levels. The hybrid functional B3LYP extends the correlation effect, as deployed by Lee, Yang, and Parr, by incorporating Becke's exchange interactions described by the exchange-correlation functional:

$$E_{\{xc\}} = aE_x^{\{HF\}} + (1-a)E_x^{\{LSDA\}} + bE_x^{\{B88\}} + cE_c^{\{LYP\}} \text{----------(1)}$$

where $E_x^{\{HF\}}$ is the Hartree-Fock exchange, $E_x^{\{LSDA\}}$ is the local spin density approximation exchange, $E_x^{\{B88\}}$ is the Becke 1988 exchange, and $E_c^{\{LYP\}}$ is the Lee-Yang-Parr correlation functional [9-11]. The ability of the B3LYP hybrid functional to accurately model the electronic structure of the molecule under investigation was facilitated by these elements.

Two specialized software programs were used to analyze the various aspects of the molecular structure. These programs were used to visualize the surface electrostatic potential (ESP) and calculate the total, partial, and overlap density of states. In addition, they were used to compute the reduced density gradient (RDG), electron localization function (ELF), and localized orbital locator (LOL). The first analysis tool available in the Multiwfn program allows users to investigate the properties of multiple molecular systems. The reduced density gradient (RDG) was calculated using the following equation.

$$RDG(r) = \frac{1}{2(3\pi^2)^{\frac{1}{3}}} \left|\frac{\nabla\rho(r)}{\rho(r)}\right|^{\frac{4}{3}} \text{--------} \quad (2)$$

where $\rho(r)$ is the electron density at position and $\nabla\rho(r)$ represents its gradient [12]. VMD operates as a complete program that enables users to analyze and visualize the outputs from molecular dynamics simulations [13,14].

The ultraviolet-visible (UV-Vis) absorption spectrum was used to investigate the electronic transitions occurring within the molecular orbitals. This analysis was conducted employing the 6-311++G(d,p) basis set, B3LYP hybrid functional, and time-dependent DFT (TD-DFT). The electronic excitation energies were determined using the solution of the linear response equation:

$$(H - E_{kS})C_k = 0 \text{ --------(3)}$$

where H is the Hamiltonian matrix, S is the overlap matrix, E_K is the excitation energy, and C_K is the eigenvector coefficient [15,16]. Through theoretical analysis, we obtained an accurate characterization of the electronic properties and transitions of carbonofluoridic acid in different environments, thereby providing a full photophysical understanding. The three Fukui functions that represent distinct approaches to chemical attack are nucleophilic $f^+(\vec{r})$, electrophilic $f^-(\vec{r})$, and radical$f^0(\vec{r})$. The functions analyze the electron density prospects for molecular reactivity through reaction analysis of radical, electrophilic, and nucleophilic attack modes. The following mathematical formulae establish the calculation method for determining these values.

$$f^+(\vec{r}) = q_r(N+1) - q_r(N) \quad \text{---------} \quad (4)$$

$$f^-(\vec{r}) = q_r(N) - q_r(N-1) \quad \text{----------} \quad (5)$$

$$f^0(\vec{r}) = \frac{q_r(N+1) - q_r(N-1)}{2}) \quad \text{----------} \quad (6)$$

Where, the values of $\boldsymbol{f^+(\vec{r})}$ and $\boldsymbol{f^-(\vec{r})}$ indicate an atom's capacity to acquire an additional electron or deal with losing one electron and $\boldsymbol{f^0(\vec{r})}$ indicates radical reactivity. The dual descriptor $\Delta \boldsymbol{f}(\vec{r})$ is an essential computational tool that provides important information about a molecule's reactivity by measuring the difference between the electrophilic and nucleophilic Fukui functions. The identification of specific molecular sites targeted by electrophiles or nucleophiles aids in their recognition. This is essential for anticipating reaction mechanisms and creating compounds capable of selectively interacting with reactive entities across various chemical and biological systems.

$$\Delta \boldsymbol{f}(\vec{r}) = \boldsymbol{f^+(\vec{r})} - \boldsymbol{f^-}(\vec{r}) \quad \text{----------} \quad (7)$$

where $\Delta \boldsymbol{f}(\vec{r}) > \mathbf{0}$ indicates a nucleophilic attack, and $\Delta \boldsymbol{f}(\vec{r}) < \mathbf{0}$ indicates electrophilic attacks. The electrophilic and nucleophilic attack equations were averaged to determine the final equation for the radical attack. Therefore, the most reactive electrophilic and nucleophilic sites in the reagent could be identified using a single quantity$\Delta \boldsymbol{f}(\vec{r})$. A positive $\Delta \boldsymbol{f}(\vec{r})$ indicates a nucleophilic attack, whereas a negative $\Delta \boldsymbol{f}(\vec{r})$ indicates an electrophilic attack. This study adopted the 6-311++G(d,p) basis set together with the B3LYP hybrid functional and TD-DFT to precisely examine the reactiveness of the molecule [17-19].

In addition, the FT-Raman intensity and FT-IR absorption of the optimized structure were calculated using the Gaussian software. The thermochemical characteristics of carbonofluoridic acid were assessed using quadratic equations and the Moltran software. The thermodynamic functions, including Gibbs free energy (G), enthalpy (H), and entropy (S), were derived using standard thermodynamic relations:

$$\boldsymbol{G = H - TS} \quad \text{---------} \quad (8)$$

$$\boldsymbol{dG = VdP - SdT} \quad \text{----------} \quad (9)$$

These computations offer an essential understanding of the stability and reactivity of the molecule under different conditions [20].

Results and Discussion

Optimized Molecular Geometry

The geometrical optimization energies of the title molecule were computed using the B3LYP/6-311G++(d,p) basis set in the Gaussian 09 W and GaussView software. The optimized geometrical structure is illustrated in **Figure.1**. The molecule under investigation consisted of 32 electrons and 5 atoms. Total energy calculations were performed through geometric optimization, which involved adjusting the carbonofluoridic acid bond lengths, angles, and dihedral angles while integrating fluorine and oxygen with carbon. Energy minimization is crucial for determining the lowest-energy configuration and establishing stable structural coordinates. Zero charge was maintained during the Gaussian

computation [21]. The geometric properties, including the torsion angles, bond lengths, and bond angles, are listed in **Table 1**. The molecular structure was further refined by energy minimization using the Gaussian method to ensure its stability and accuracy [22].

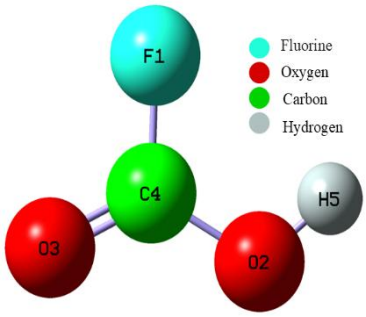

Figure 1: Optimized structure of the title molecule

Table 1: Calculated bond lengths (Å), bond angles (°) and torsion angles (°) for the title molecule

Atoms	Bond length (Å)	Atoms	Bond angle (°)	Atoms	Torsion angles (°)
C4–O2	1.35342	C4–O2–H5	113.360	F1–C4–O2–H5	0.01630
C4–F1	1.42872	F1–C4–O3	108.653	O3–C4–O2–H5	179.946
C4–O3	1.19890	O2–C4–O3	128.802		
O2–H5	0.99622	F1–C4–O3	122.543		

HOMO-LUMO Gap Calculation and Chemical Reactivity

The title molecule exhibits chemical reactivity owing to its distinct frontier molecular orbital properties. The calculated HOMO-LUMO gap, which indicates the electronic excitation potential of the molecule was 8.68708 eV. This value suggests high stability and low reactivity, as evidenced owing to the substantial energy barrier for the electronic transitions.The transition from the ground state to the first excited state occurs when an electron moves from the highest occupied molecular orbital (HOMO) to the lowest unoccupied molecular orbital (LUMO). This process is known as the electron excitation. A reduced HOMO-LUMO energy gap facilitates this excitation, promoting intercharge transformation and influencing the bioactivity of the biomolecules.

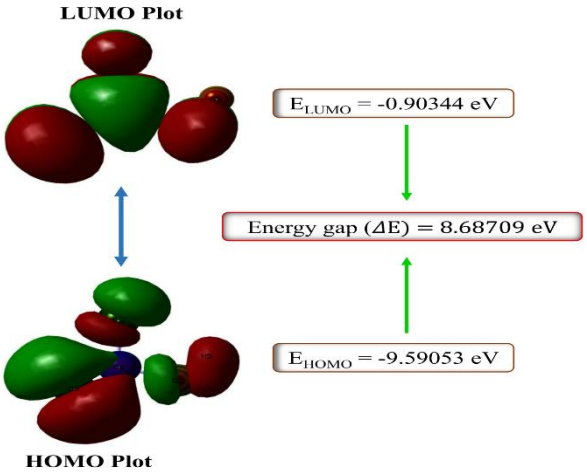

Figure 2: The molecular orbitals and energies for the HOMO and LUMO of title molecule.

Conversely, an increased energy band gap results in enhanced kinetic stability and diminished chemical reactivity owing to the increased resistance to electron removal from the lower-lying HOMO and electron addition to the higher-lying LUMO [23]. **Figure 2** shows an energy level diagram of the frontier orbitals of the carbonofluoridic acid molecule. The HOMO and LUMO energies were determined to be -9.59053 eV and -0.90344 eV, respectively, resulting in an energy gap of 8.68709 eV. Such a large gap suggests minimal electron delocalization and limited reactivity [24, 25].

Global Reactivity Index (GRI) Calculations

The global reactivity index (GRI) is a set of parameters utilized in solid-state physics and quantum chemistry that combines a molecule's electrophilicity, hardness, and chemical potential to ascertain its reactivity. This index serves to predict the stability and overall chemical behavior of a reaction. **Table 2** lists the calculated electronic descriptors of the title molecule. The relatively high chemical hardness of 4.34354 eV suggests diminished reactivity.

Table 2: Calculated global reactivity index of carbonofluoridic acid.

Global reactivity descriptor	Equations	Values
E_{HOMO}	- -	-9.59053 eV.
E_{LUMO}	- -	-0.90344 eV
Energy gap ΔE	$\Delta E = E_{LUMO}-E_{HOMO}$	8.68709 eV
Ionization energy (I)	- -	9.59053 eV
Electron affinity (A)	- -	0.90344 eV
Chemical hardness (η)	$(\eta) = \frac{(I-A)}{2}$	4.34354 eV
Global softness (S)	$(S) = \frac{1}{\eta}$	0.23023 eV^{-1}
Nucleofugality (ΔEn)	$\Delta En = \frac{(\mu+\eta)^2}{2\eta}$	0.11511 eV^{-1}
Global electrophilicity index (ω)	$(\omega) = \frac{\mu^2}{2\eta}$	0.09396 eV
Electronegativity (χ)	$(\chi) = \frac{(I+A)}{2}$	3.16917 eV
Chemical potential (μ)	$(\mu) = -\frac{(I-A)}{2}$	-5.24698 eV
Electrofugality (ΔEe)	$\Delta Ee = \frac{(\mu-\eta)^2}{2\eta}$	10.58793 eV

The electronegativity value of 5.24698 eV contributes to the elevated charge flow owing to the pronounced electron-attracting capacity of the molecule. The electronegativity value of 5.24698 eV contributes to the elevated charge flow owing to the pronounced electron-attracting capacity of the molecule. The high electrophilicity index indicates a significant energy reduction associated with maximal electron flow between the donor (HOMO) and acceptor (LUMO), facilitating electron release in charge-transfer reactions, as evidenced by its high electrofugality. The approximate nucleofugality suggests its potential utility as a leaving group in nucleophilic substitutions [26]. The electronic descriptors listed in **Table 2** elucidate the reactivity and interaction potential of the title molecule in a chemical system.

Molecular Electrostatic Potential (MEP)

Figure 3 displays the molecular electrostatic potential (MEP) along with its corresponding contour map, which was created using GaussView and Gaussian09 with the DFT/B3LYP/6-311++G(d,p) basis set. MEP surfaces display varying potential colors from red (strongest repulsion) to blue (strongest attraction) [27]. The gas-phase MEP surface of carbonofluoridic acid (**Figure 3 (a)**) exhibited potential values ranging from -8.843×10^{-3} a.u. (red, negative region) to $+8.843\times10^{-3}$ a.u. (blue, positive region).

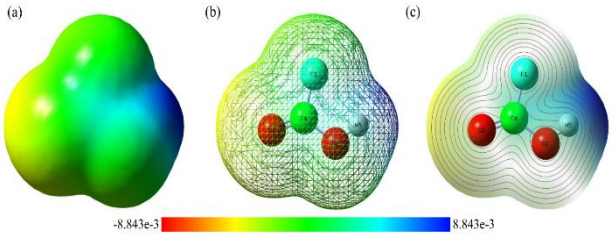

Figure 3: (a) Solid view (b) Mesh view, and (c) MEP surface map with the contour lines of the title molecule

This visualization revealed a significant negative potential around the oxygen atoms and a positive potential near the hydrogen atoms, indicating reactive sites. MEP surfaces generally exhibit a preference for positive regions for nucleophilic attacks and negative regions for electrophilic attacks. **Figure 3(c)** illustrates the electron density obtained from the total self-consistent field (SCF) density using MEP. The highest negative MEP regions were primarily located on oxygen atoms from the C=O and C-O bonds, indicating potential sites for electrophilic attack. Conversely, the most positive MEP regions were observed across hydrogen atoms in the O-H group. Carbon atoms exhibit neutral or slightly positive MEP, particularly when bound to hydrogen or other carbon atoms. This can be attributed to their similar electronegativities, which results in a more equitable electron distribution in the bonds. The oxygen atoms (O2 and O3) were surrounded by areas of high electrostatic potential, which is indicative of repellent interactions. In contrast, a particular hydrogen atom (H5) exhibits areas of stronger attraction. The fluorine atom (F1) is less attractive and contributes to the overall stability of the molecule [28].The

understanding of a molecule's polarity, reactivity, chemical behavior, and potential for interactions with other molecules is dependent on its MEP, which provides a visual representation of its electrostatic environment.

Total, Partial and Overlap Density of States Analysis

The energy level distribution is presented in the density of states (DOS) diagram in **Figure.4**. Through partial density of states (PDOS) analysis, the density contributions from individual fragment orbitals were integrated to determine the total density of states (TDOS).

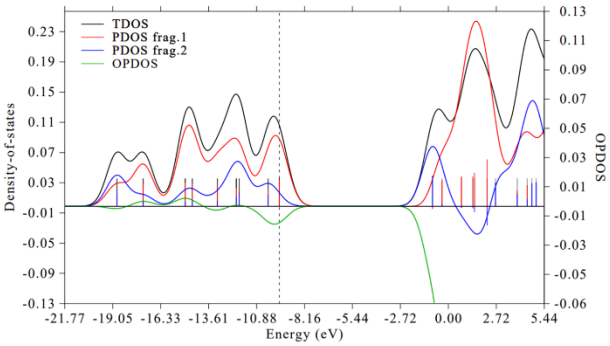

Figure 4: The spectral graph that illustrates the TDOS, PDOS and OPDOS for the title molecule

The TDOS graph is depicted as a black line generated by Multiwfn software. **Figure.4** presents plots of the total, partial, and overlap population densities of states (TDOS, PDOS, and OPDOS, respectively) for carbonofluoridic acid. The molecule was divided into two fragment groups: f1 (carbonyl group) and f2(hydroxyl group). The resulting graph illustrates the molecular orbital (MO) composition and its significance in chemical bonding. The OPDOS depicts the bonding, anti-bonding, and non-bonding characteristics of the interaction between orbitals, atoms, or groups. The diagram of carbonofluoridic acid total electronic density of states (TDOS) is depicted by the black line in the graph [29].The vertical dashed line represents the HOMO energy level, which denotes the highest energy orbital containing electrons in a molecule during its ground-state configuration. The PDOS of fragments 1 and 2 are depicted by red and blue curves and discrete lines, respectively [30]. The overlap density of states, or OPDOS, is illustrated by the green curve on the right side of the Y-axis and is set to -0.06–0.13.

Spectroscopic Analysis

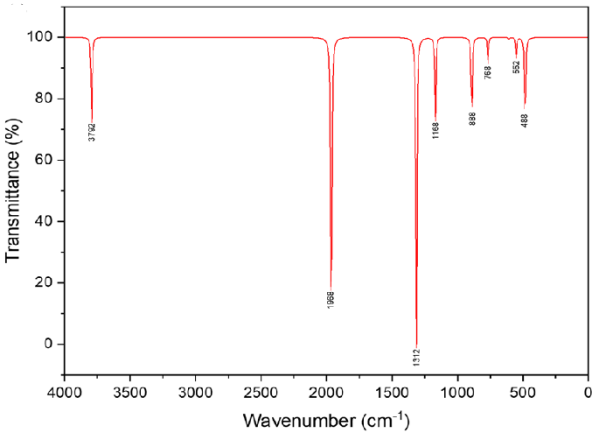

Figure 5: FT-IR spectra

When analyzed using Fourier transform infrared (FT-IR) and Fourier transform Raman (FT-Raman) spectroscopic methods, the compound being investigated displayed characteristic vibrational patterns within the 4000 to 0 cm^{-1} range. These patterns are associated with the stretching vibrations of the functional O−H, C=O, C−O, and C−F groups [31]. The advanced techniques of FT-IR and FT-Raman spectroscopy were employed to investigate the vibrational modes of molecules and provide additional information about the molecular structure of a sample. FT-IR quantifies the amount of infrared light absorbed by a sample, which is equivalent to the vibrational frequencies of molecular bonds. This provides information about the molecular interactions, bond strengths, and functional groups. Conversely, FT-Raman detects Raman scattering, wherein vibrational transitions become visible owing to the inelastic scattering of light by the molecules. The results of FT-IR and FT-Raman spectroscopy, which provide details on the molecular composition of the title molecule and elucidate its vibrational spectra, are presented in **Figure 5** and **Figure 6**,

respectively [32].

O–H stretching vibration

The O–H bonds found in all hydrocarbons ranged in length from 3600 to 3200 cm^{-1}. Furthermore, the vibrational frequency of free OH – ions, which cannot be measured directly, has been reported to be 3700 cm^{-1}. The FT-IR spectrum of the title molecule shows an O – H stretching vibration at 3792 cm^{-1}. Likewise, the Raman spectrum reveals an O – H stretching vibration at the same frequency of 3792 cm-1. The most significant peak in the transmittance band, as depicted in **Figure.6**, corresponds to the O – H stretching mode in the Raman spectrum.Notably, both FT-IR and FT-Raman measurements of the O–H stretching vibrations yielded identical values. The O–H out-of-plane bending is responsible for these exceptionally strong and weak infrared intensities [33]. The position and shape of this peak provide critical information about the molecular environment, strength of hydrogen bonds, and overall structure of the molecule.

C=O stretching vibration

This stretching mode exhibited a single peak associated with the carbonyl (C=O) group in the infrared (IR) intensity transmittance band range, typically occurring within the 1650–1850 cm^{-1} range. The C=O vibration of the investigated molecule was observed at 1968 cm^{-1}. In Raman spectroscopy, the C=O vibration was also detected at 1968 cm^{-1}In this case, both Fourier transform infrared (FT-IR) and Fourier-transform Raman (FT-Raman) spectroscopic techniques provided similar measurements for C=O stretching vibrations [34].

C–O vibration

C–O vibrations typically occur in the range of 1260-1000 cm^{-1}. In the FT-IR spectra, the C–O stretching vibration bands are observed in the 1312, 1668 cm-1 region. Intense peaks were detected in the FT-IR carbonofluoridic acid absorption bands associated with C – O bond bending owing to the substantial dipolar shift in that specific mode. In FT-Raman, the C–O stretching vibration has also been observed in the same vibrational region as in FT-IR. Additionally, measurements were conducted in the 552 and 488 cm^{-1} regions for C–O and C=O vibrations using FT-IR and FT-Raman spectroscopy. These vibrational modes encompass bending, twisting, and lattice vibrations, and are frequently associated with functional groups and bonds [33, 35].

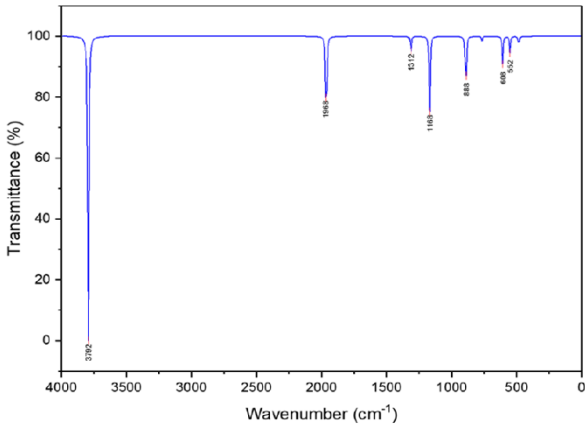

Figure 6: FT-RAMAN spectra of the title molecule

C–F vibration

The C—F vibration range of the molecule under investigation is 600—900 cm^{-1}. In FT-IR spectroscopy, wavenumbers of approximately 888 cm^{-1} and 768 cm^{-1} are typically within the range of C-F (carbon-fluorine) vibrations. The C-F stretching vibrations generally manifest between 888 and 608 cm^{-1} in FT-Raman spectroscopy. These peaks indicate the presence of carbon-fluorine bonds in carbonofluoridic acid. FT-IR and FT-Raman spectroscopies function complementarily to identify and validate functional groups and their interactions, thereby contributing to a comprehensive understanding of the molecular structure of carbonofluoridic acid [36,37].

UV-vis Spectra Analysis

Ultraviolet-visible (UV-Vis) spectral analysis is a technique used to measure the absorption of visible and ultraviolet light by a substance. Time-dependent functional theory

(TD-DFT) utilizing the TD-SCF/6-311++G (d,p) method was employed to calculate the UV-vis spectra and characteristics, including electronic transitions and excitation energy-optimized structures, which exhibit a very weak oscillator. Consequently, the absorption is likely to be significantly weaker [38]. **Figure.7** shows that the maximum wavelength in the neutral state was 173.92 nm. The comprehensive information provided by the UV-vis spectral analysis of electronic transitions in molecules facilitates the understanding of molecular interactions, identification of functional groups, and determination of molecular structure. It has been extensively employed for both qualitative and quantitative analyses across numerous scientific disciplines including chemistry, biology, and physics.

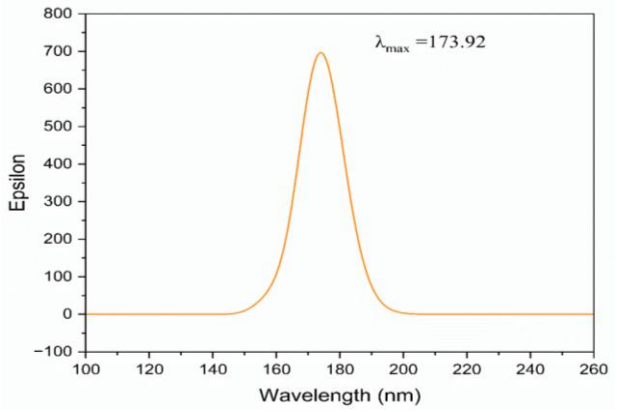

Figure 7: UV-vis Spectrum of the title molecule

Thermochemical Calculations

The thermochemical parameters increase between 50 and 500 K because the vibrational intensities of the molecules increase with temperature. Thermochemical analysis of the target molecule was performed using statistical methods at a standard room temperature (298.15 K) and atmospheric pressure. The enthalpy, entropy, and heat capacity at constant pressure were calculated using specific equations for a range of temperatures. These thermodynamic properties, which can be calculated using the equations provided over a range of temperatures, are essential for understanding and predicting the behavior of substances in a variety of thermodynamic processes. In some circumstances, it is possible to model the relationship between the heat capacity, entropy, and enthalpy with regard to temperature changes using a quadratic equation. This is frequently relevant when the temperature-dependent variation in heat capacity (C_p) can be roughly described by a quadratic equation [39].

$$S\ (T) = -2.51756\times10^{-4}\ T^2 + 3.48517\times10^{-1}\ T + 1.87405\times10^{2} \quad (10)$$

$$H\ (T) = 5.23393\times10^{-5}\ T^2 + 2.24579\times10^{-2}\ T + 6.95423\times10 \quad (11)$$

$$C_p\ (T) = 1.34634\times10^{-5}\ T^2 + 8.60477\times10^{-2}\ T + 2.64690\times10 \quad (12)$$

Table 3. Thermodynamic properties of the carbonofluoridic acid at different temperatures

Temperature (K)	Cp (J/K/mol)	H (kJ/mol)	S (J/K/mol)
50	30.8050	70.7960	204.201
100	35.2084	72.3114	219.739
150	39.6790	74.0886	234.018
200	44.2170	76.1274	247.038
250	48.8223	78.4279	258.799
298.15	53.3068	80.8826	268.906
300	53.4950	80.9902	269.302
350	58.2349	83.8141	278.545
400	63.0422	86.8997	286.530
450	67.9168	90.2470	293.257
500	72.8587	93.8560	298.724

The thermochemical parameters in **Table 3** exhibit a consistent increase with temperature from 50 to 500 K and plotted in **Figure.8**, indicating a correlation between the temperature and thermodynamic properties. The entropy (S) increased from 204.201 J/K/mol at 50 K to 298.724 J/K/mol at 500 K, reflecting increased system disorder. The heat capacity at a constant pressure (Cp) increased from 30.8085 to 72.8587 J/K/mol, demonstrating an enhanced heat absorption capacity. The enthalpy (H) increased from

70.7960 to 93.8560 kJ/mol, which is consistent with the increased internal energy and molecular excitation. These trends provide insights into the thermal properties and responsiveness of the material, which are characteristic of carbonofluoridic acid behavior under thermal conditions.

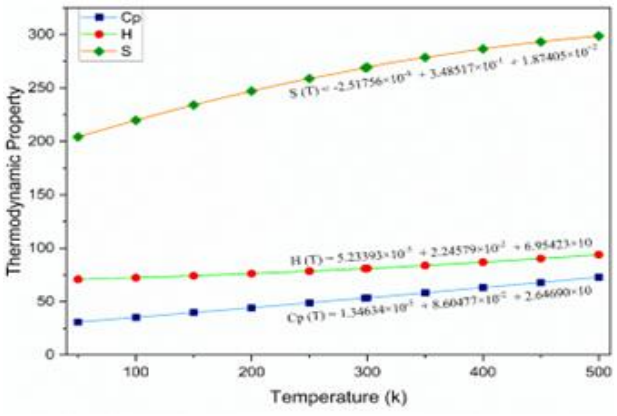

Figure 8: Variation in entropy (S), enthalpy (H), and heat capacity (C_p) in J/K/mol with temperature.

Reduced Density Gradient (RDG) Analysis and its Implications

Reduced density gradient (RDG) is a methodology employed in quantum chemistry to investigate non-covalent molecular interactions. These interactions, which encompass hydrogen bonds, steric repulsion, and van der Waals forces, are crucial for understanding the molecular behavior, particularly in chemical and biological reactions. RDG identifies molecular interactions by quantifying electron density and its gradients. The RDG equation normalizes the density gradient, which facilitates the examination and visualization of weak interactions within molecular systems [40]. RDG analysis of the carbonofluoridic acid 3D RDG plot is shown in **Figure.9**. A scatter graph depicting the reduced density gradient (RDG) versus the electron density multiplied by the sign of the second Hessian eigenvalue was used to visualize inter- and intramolecular weak interactions, as illustrated in **Figure.9**. The color gradients (blue: ≤ -0.035 a.u., green: ~0 a.u., red: ≥ 0.015 a.u.) highlight weak interactions, such as lone-pair effects or van der Waals forces [41,42]. Fluorine's electronegativity drives electron density withdrawal from the carbon center, a phenomenon corroborated by density functional theory (DFT) studies on non-covalent interactions in similar systems [43,44].

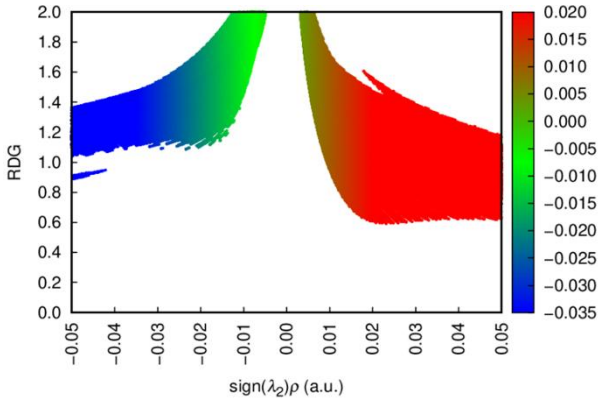

Figure 9: RDG plot of carbonofluoridic acid

Interpretations of Electron Density Distribution, Reactivity, and Localization (ELF and LOL Analysis)

The electron localization function (ELF) and localized orbital locator (LOL) are sophisticated computational tools used to investigate the electron density, bonding, and orbital interactions in molecular structures. While ELF primarily focuses on electron localization, LOL provides data on molecular orbital localization to enhance our understanding of the molecular

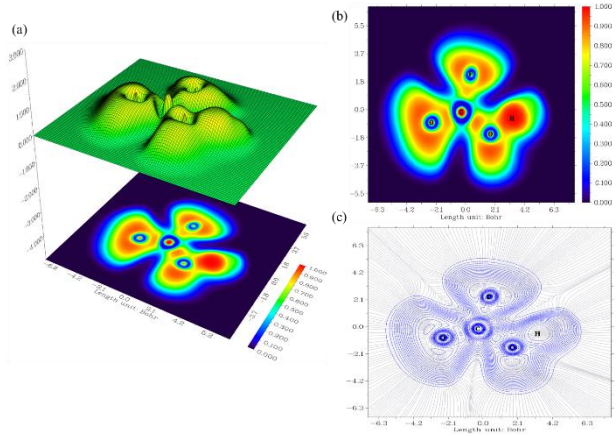

Figure 10: (a) Shaded surface map with the projection of ELF, (b) Colored surface plot for ELF and (c) Contour Mapped Surface of the Title Molecule

structure, reactivity, and stability. These tools are essential for studying chemical systems and predicting molecular behavior in fields such as materials science, drug design, and quantum chemistry. The ELF and LOL maps offer a comprehensive coverage of orbital interactions, bonding electron localization, and electron density distribution in the analysis of carbonofluoridic acid. For carbonofluoridic acid, the color-shaded and contour maps of ELF and LOL are presented in **Figures.** (**10** and **11** (**a, b, and c**)). Complex geometric structures were also generated for analysis at the B3LYP level of theory using molecular orbital analysis, Multiwfn software, and molecular electrostatic potential mapping.The ELF map was plotted within the range of 0.0 to 1.0. Bonding and nonbonding localized electrons are present in the interval of 0.5 to 1.0, whereas delocalized electrons are anticipated in the smaller interval (0.5).

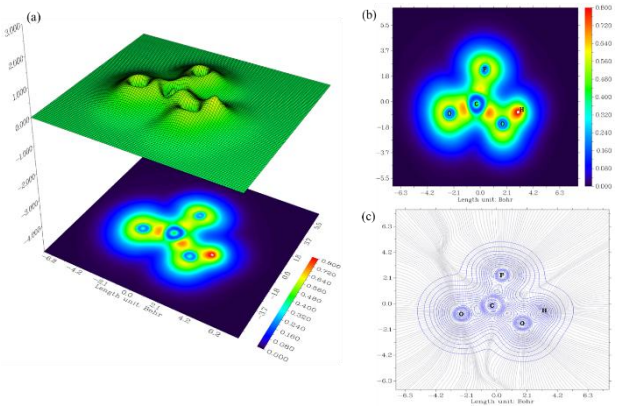

Figure 11: (a) Shaded Surface Map with Projection, (b) Color Shade Map of LOL, and (c) contour map with projection of LOL of the title molecule.

In areas where electron localization dominates the electron density, the LOL reaches high values, exceeding 0.5. The color sequence of red < orange < yellow < green < blue represents increasing values. A high value in a specific region indicates significant electron localization, which is characteristic of covalent bonds or nuclear shells. **Figure.10** illustrates both bonding and nonbonding electrons [45]. The high concentrations of these electrons, which can be attributed to the nuclear shells, lone pairs, or covalent bonds, are denoted by the red color surrounding the hydrogen atom. The blue circle around the oxygen atoms in carbonofluoridic acid represents areas of electronic depletion between the inner and valence layers, whereas the blue color around the carbon atom signifies delocalized electrons. The regions surrounding F1, O2, and O3, which formed single and double bonds with the carbon atom (C4), exhibited lower electron densities. These regions transition from red to light red and yellow at the edges.The LOL central region appears white because the electron density surpasses the upper threshold of the color scale [46]. To confirm the existence of bonding and nonbonding electrons, the LOL equation was employed to shade the ELF and LOL maps depicted in **Figure.10** and **Figure.11**.

$$LOL\ (r) = \frac{\tau(r)}{1+\tau(r)} \quad (13)$$

where τ(r) is electron density. In this study, topology analysis of the LOL was utilized to determine the location of the LOL maximum and analyze its characteristics. Notably, aromatic hydrogen atoms exhibited tightly confined electron regions, whereas carbon atoms exhibited depleted electron zones (**Figure. 11 (a), (b), and (c)**). As illustrated in **Figure.11 ((a) and (b)**), the white color at the center of the hydrogen atom (H5) indicates electron density exceeding the color scale limit (0.80) in the LOL color map. Molecular electrostatic potential mapping, MO analysis, and ELF and LOL analyses can be employed to elucidate the structural properties, reactivity, and potential interactions of the title molecule [47].

Fukui Functions and Dual Descriptors

Fukui functions are fundamental mathematical constructs that provide information regarding the propensity of a molecule to donate or accept electrons, thereby

elucidating whether an atom within a molecule exhibits electrophilic or nucleophilic characteristics. Fukui functions and dual descriptors are essential analytical tools in this domain because of their capacity to elucidate the reactivity of specific molecular sites. Density functional theory (DFT) and time-dependent density functional theory (TD-DFT) offer useful computational frameworks for examining these characteristics [48]. **Table 4** presents the specific results. Fig.12 illustrates the Fukui functions for carbonofluoridic acid and the reactivity in various atoms. Cluster analysis of the molecule showed similar patterns, and the DFT/B3LYP/6-311++G(d,p) method yielded nearly identical results. This approach demonstrates high reliability, as evidenced by the reduced dependence of Fukui reaction indices on the basis set. Atoms with a low Fukui reaction index f^+ ($r^{\rightarrow}$) exhibit decreased reactivity towards nucleophiles because of their stability in nucleophilic reactions.Fukui reaction indices f^- ($r^{\rightarrow}$) were also employed to evaluate the susceptibility of the molecule to electrophilic attack. The results presented in Figure.12 indicate that the carbonofluoridic atoms have low Fukui values.

Table 4: Fukui functions and dual descriptor calculated based on the natural population analysis (NPA) of carbonofluoridic acid

Atoms	F1	O2	O3	C4	H5
Anion (N+1)	-0.40585	-0.83272	-0.72095	1.24945	-0.28993
Neutral (N)	-0.34642	-0.66288	-0.55749	1.07136	0.49543
Cation (N-1)	-0.19045	-0.54706	0.07267	1.10298	0.56186
$f^+(r^{\rightarrow})$	-0.05943	-0.16984	-0.16346	0.17809	-0.78536
$f^-(r^{\rightarrow})$	-0.15597	-0.11582	-0.63016	-0.03162	-0.06643
$f^0(r^{\rightarrow})$	-0.10770	-0.14283	-0.39681	0.07323	-0.42590
$\Delta f(r^{\rightarrow})$	0.09654	-0.05402	0.46670	0.20971	-0.71893

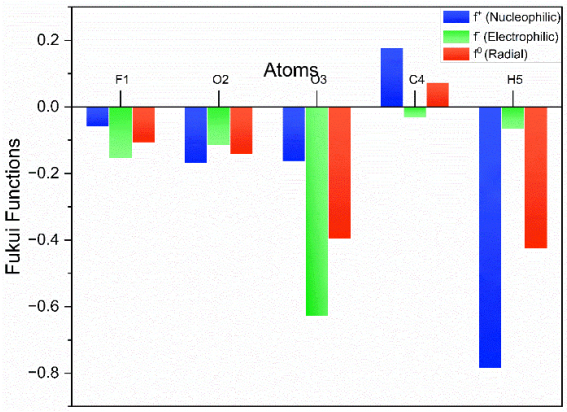

Figure 12: Fukui Functions with neutral, positive, and negative values of the title molecule

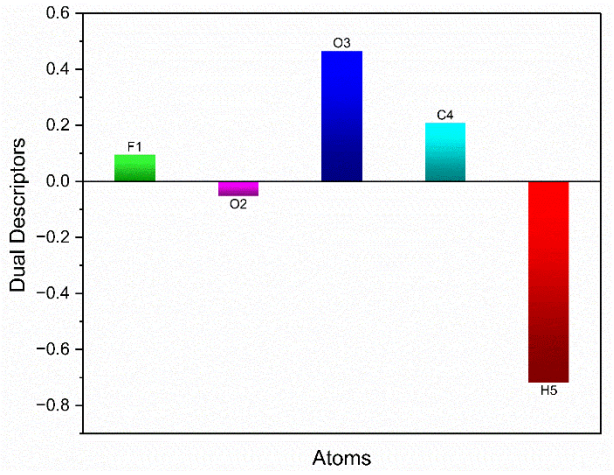

Figure 13: Plotted chart of dual descriptor of the title molecule

Consequently, carbonofluoridic atoms demonstrate reduced reactivity with electrophiles. These two Fukui reaction indices can be utilized to assess the stability of an atom in both electrophilic and nucleophilic reactions. Furthermore, dual analysis facilitates the prediction and comprehension of the reactivity of a molecule by identifying its reactive sites and providing insights into its chemical behavior.**Figure.13** presents a dual-descriptor plot in accordance with **Table 4**. The title molecule exhibited electrophilic susceptibility to O2 along with H5 atoms, and nucleophilic susceptibility to F1, O3, and C4. This information is valuable for predicting the molecular behavior in various contexts, particularly when interacting with both

electrophilic and nucleophilic reagents. Furthermore, it provides insights into designing reactions that specifically target these critical sites for effective drug development and chemical synthesis [49].Specific sites that exhibited increased susceptibility to electrophilic or nucleophilic attacks were identified, providing critical information about the potential behavior of the molecule in chemical reactions. This knowledge will facilitate the development of more efficient and precise synthetic and medicinal chemistry techniques.

Conclusions

This study comprehensively investigated the structural, electronic, and reactivity characteristics of a title molecule using DFT-based computational techniques. The optimized geometrical structure, along with its HOMO-LUMO energy gap, suggested a highly stable molecular framework with minimal chemical reactivity. The global reactivity indices reinforce this observation, indicating significant resistance to charge transfer. MEP analysis identified crucial reactive sites, whereas ELF and LOL mapping confirmed electron density localization, signifying strong covalent interactions. RDG analysis provides insights into non-covalent interactions, thereby supplementing our understanding of molecular stability. Fukui function and dual descriptor evaluations pinpoint electrophilic and nucleophilic attack regions, aiding chemical reactivity predictions.Spectroscopic analysis further validated the molecular vibrational characteristics, supporting structural integrity. The TDOS, PDOS, and OPDOS calculations confirmed the orbital contributions and electronic transitions. These findings not only enhance the understanding of the electronic behavior of the title molecule, but also pave the way for its potential applications in medicinal chemistry, nanomaterials, and catalysis. Future work may involve experimental validation and exploration of solvent effects to extend the applicability of the computational insights.

Acknowledgements

We sincerely thank the professors from the Central Department of Physics and the Department of Physics at the Patan Multiple Campus for their invaluable support.

Author's Contribution Statement

K. Basnet: Conceptualization, Methodology, Data Curation, Resources, Software, Investigation, Writing - Original Draft, **B. Neupane:** Conceptualization, Methodology, Formal analysis, Editing, Validation, Visualization, Writing - Original Draft.

Conflict of Interest

The authors declare that they have no conflicts of interest throughout this research work.

Data Availability Statement

The data supporting the findings of this study are available from the corresponding authors upon reasonable request.

References

1 B. Bauer, S. Bravyi, M. Motta and G. K. L. Chan, Quantum algorithms for quantum chemistry and quantum materials science, *Chemical Reviews*, 2020, 120(22), 12685-12717. (https://doi.org/10.1021/acs.chemrev.9b00829)

2. G. O. Jones, A. Yuen, R. J. Wojtecki, J. L. Hedrick and J. M. Garcia, Computational and experimental investigations of one-step conversion of poly(carbonate) into value-added poly(aryl ether sulfone), *Proceedings of the National Academy of Sciences*, 2016, 113(28), 7722–7726. (https://doi.org/10.1073/pnas.1600924113)

3. T. Aggarwal and A. K. Verma, Achievements in fluorination using various reagents through deoxyfluorination, *Organic Chemistry Frontiers*, 2021, 8(22), 6452–6468. (https://doi.org/10.1039/D1QO00952D)

4. H. X. Song, Z. Y. Tian, J. C. Xiao and C. P. Zhang,

Tertiary-amine-initiated synthesis of acyl fluorides from carboxylic acids and $CF_3SO_2OCF_3$, *Chemistry – A European Journal*, 2020, 26(69), 16261–16265. (https://doi.org/10.1002/chem.202003756)

5. R. Tafrishi, D. Torres-Diaz, L. Amiaud, A. Lafosse and O. Ingólfsson, Low-energy electron interactions with 2-(trifluoromethyl) acrylic acid are a potential component of EUVL resist materials, *Physical Chemistry Chemical Physics*, 2023, 25(27), 17987–17998. (https://doi.org/10.1039/D3CP01860A)
6. P. Hohenberg and W. Kohn, Inhomogeneous electron gas, *Physical Review*, 1964, 136(3B), B864. (https://doi.org/10.1103/PhysRev.136.B864)
7. M. J. Frisch et al., Gaussian 09, Revision D.01, Gaussian Inc., Wallingford, CT, 2009.
8. R. D. Dennington II, T. A. Keith and J. M. Millam, GaussView, Version 6.0.16, Semichem Inc., Shawnee Mission, KS, 2016.
9. C. Lee, W. Yang and R. G. Parr, Development of the Colle-Salvetti correlation-energy formula into a functional of electron density, *Physical Review B*, 1988, 37(2), 785. (https://doi.org/10.1103/PhysRevB.37.785)
10. A. D. Becke, Density-functional thermochemistry. III. Role of exact exchange, *The Journal of Chemical Physics*, 1993, 98(7), 5648–5652. (https://doi.org/10.1063/1.464913)
11. T. H. Dunning Jr, Gaussian basis sets for correlated molecular calculations. I. The atoms boron through neon and hydrogen, *The Journal of Chemical Physics*, 1989, 90(2), 1007–1023. (https://doi.org/10.1063/1.456153)
12. N. Shanmugapriya, V. Balachandran, B. Revathi, B. Narayana, V. V. Salian, K. Vanasundari and C. Sivakumar, Quantum chemical calculation, performance of selective antimicrobial activity using molecular docking analysis, RDG and experimental (FT-IR, FT-Raman) investigation of 4-[{2-[3-(4-chlorophenyl)-5-(4-propan-2-yl) phenyl)-4,5-dihydro-1H-pyrazol-1-yl]-4-oxo-1,3-thiazol-5(4H)-ylidene} methyl] benzonitrile, *Heliyon*, 2021, 7(7). (http://doi.org/10.1016/j.heliyon.2021.e07634)
13. T. Lu and F. Chen, Multiwfn: A multifunctional wavefunction analyzer, *Journal of Computational Chemistry*, 2012, 33(5), 580. (https://doi.org/10.1002/jcc.22885)
14. W. Humphrey, A. Dalke and K. Schulten, VMD: Visual Molecular Dynamics, *Journal of Molecular Graphics*, 1996, 14(1), 33–38. (10.1016/02637855(96)00018-5)
15. M. Cossi, G. Scalmani, N. Rega and V. Barone, New developments in the polarizable continuum model for quantum mechanical and classical calculations of molecules in solution, *The Journal of Chemical Physics*, 2002, 117(1), 43–54. (https://doi.org/10.1063/1.1480445)
16. R. E. Stratmann, G. E. Scuseria and M. J. Frisch, Efficient implementation of time-dependent density functional theory for the calculation of the excitation energies of large molecules, *The Journal of Chemical Physics*, 1998, 109(19), 8218–8224. (https://doi.org/10.1063/1.477483)
17. P. P. Zamora, K. Bieger, A. Cuchillo, A. Tello and J. P. Muena, Theoretical determination of a reaction intermediate: Fukui function analysis, dual-reactivity descriptor, and activation energy, *Journal of Molecular Structure*, 2021, 1227, 129369. (10.1016/j.molstruc.2020.129369)
18. J. Sánchez-Márquez, New advances in conceptual-DFT: An alternative way to calculate the Fukui function and dual descriptor, *Journal of Molecular Modeling*, 2019, 25, 1–7. (https://doi.org/10.1007/s00894-019-4000-0)
19. F. Guégan, L. Merzoud, H. Chermette and C. Morell, A perspective on the so-called dual descriptor, Chemical Reactivity in Confined Systems: *Theory, Modelling and Applications, 2021*, pp. 99–112. (https://doi.org/10.1002/9781119683353.ch6)

20. S. K. Ignatov, Moltran v.2.5 – Program for molecular visualization and thermodynamic calculations, University of Nizhny Novgorod, 2004.
21. R. Meyer and A. W. Hauser, Geometry optimization using Gaussian process regression in internal coordinate systems, *The Journal of Chemical Physics*, 2020, 152(8). (https://doi.org/10.1063/1.5144603)
22. P. McCabe, O. Korb and J. Cole, Kernel density estimation applied to the bond length, bond angle, and torsion angle distribution, *Journal of Chemical Information and Modeling*, 2014, 54(5), 1284–1288. (https://doi.org/10.1021/ci500156d)
23. B. G. Kim, X. Ma, C. Chen, Y. Ie, E. W. Coir, H. Hashemi, J. Kim, Energy level modulation of HOMO, LUMO, and band-gap in conjugated polymers for organic photovoltaic applications, *Advanced Functional Materials*, 2013, 23(4), 439–445. (https://doi.org/10.1002/adfm.201201385)
24. M. Miar, A. Shiroudi, K. Pourshamsian, A. R. Oliaey and F. Hatamjafari, Theoretical investigations on the HOMO–LUMO gap and global reactivity descriptor studies, natural bond orbital, and nucleus-independent chemical shifts analyses of 3-phenylbenzo[d]thiazole-2(3H)-imine and its para-substituted derivatives: Solvent and substituent effects, *Journal of Chemical Research*, 2020, 45(1–2), 147–158. (https://doi.org/10.1177/1747519820932091)
25. N. Masnabadi, M. R. Thalji, H. S. Alhasan, Z. Mahmoodi, A. V. Soldatov and G. A. Ali, Structural, electronic, reactivity, and conformational features of 2,5,5-trimethyl-1,3,2-diheterophosphinane-2-sulfide, and its derivatives: DFT, MEP, and NBO calculations, *Molecules*, 2022, 27(13), 4011. (https://doi.org/10.3390/molecules27134011)
26. S. Manivarman and S. Subashchandrabose, Synthesis and molecular characterization of pyrimidine derivatives: Combined experimental and theoretical investigation, Karbala *International Journal of Modern Science*, 2017, 3(1), 18–28. (10.1016/j.kijoms.2017.01.001)
27. S. Silvarajoo et al., Theoretical molecular electrostatic potential (MEP), highest occupied molecular orbital–lowest unoccupied molecular orbital (HOMO–LUMO) band gap, and experimental Cole–Cole plot of 4-(ortho-, meta-, and para-fluorophenyl) thiosemicarbazide isomers, *Data in Brief*, 2020, 32, 106299. (https://doi.org/10.1016/j.dib.2020.106299)
28. M. Khadka et al., Spectroscopic, quantum chemical, and topological calculations of phenylephrine molecules were performed using density functional theory, *Scientific Reports*, 2025, 15(1), 208. (10.1038/s41598-024-81633-2)
29. M. Saranya, S. Ayyappan, R. Nithya, R. K. Sangeetha and A. Gokila, Molecular structure, NBO, and HOMO-LUMO analysis of quercetin on single-layer graphene using density functional theory, *Digest Journal of Nanomaterials and Biostructures*, 2018, 13, 97–105.
30. A. Joseph, V. I. Thomas, G. Żyła, A. S. Padmanabhan and S. Mathew, Theoretical probing of weak anion–cation interactions in certain pyridinium-based ionic liquid ion pairs and the application of molecular electrostatic potential in their ionic crystal density determination: A comparative study using a density functional approach, T*he Journal of Physical Chemistry A*, 2018, 122(1), 328–340. (https://doi.org/10.1021/acs.jpca.7b09189)
31. M. Karabacak, E. Kose, E. B. Sas, M. Kurt, A. M. Asiri and A. Atac, DFT calculations and experimental FT-IR, FT-Raman, NMR, and UV–Vis spectral studies of 3-fluorophenylboronic acid, *Spectrochimica Acta Part A: Molecular and*

Biomolecular Spectroscopy, 2015, 136, 306–320. (https://doi.org/10.1016/j.saa.2014.08.141)

32. G. Socrates, *Infrared and Raman characteristic group frequencies: Tables and charts*, John Wiley & Sons, 2004.
33. M. Selvakumar and M. Vasanthy, *Innovative use of traditional seeds for drinking water purification, in Wastewater Recycling and Management: 7th IconSWM – ISWMAW 2017*, Vol. 3, Springer Singapore, 2019, pp. 285–304. (https://doi.org/10.1007/978-981-13-2619-6_22)
34. W. Xu, Y. Sun, X. Dong, S. Li, H. Wang, J. Xue and X. Zheng, Local order and vibrational coupling of the C=O Stretching mode of γ-caprolactone in liquid binary mixtures, *Scientific Reports*, 2017, 7(1), 12182. (https://doi.org/10.1038/s41598-017-12030-1)
35. S. M. Moosavinejad, M. Madhoushi, M. Vakili and D. Rasouli, Evaluation of the degradation of chemical compounds in wood in historical buildings using FT-IR and FT-Raman vibrational spectroscopy, Maderas. *Ciencia y tecnología*, 2019, 21(3), 381–392. (http://dx.doi.org/10.4067/S0718-221X2019005000310)
36. S. J. Mary, M. U. M. Siddique, S. Pradhan, V. Jayaprakash and C. James, The molecular structure, NBO analysis of the hydrogen-bonded interactions, spectroscopic (FT–IR, FT–Raman), drug likeness, and molecular docking of the novel anti COVID-19 molecule 2-[(4,6-diaminopyrimidin-2-yl) sulfanyl]-N-(4-fluorophenyl) acetamide dimer, *Spectrochimica Acta Part A: Molecular and Biomolecular Spectroscopy*, 2021, 244, 118825. (https://doi.org/10.1016/j.saa.2020.118825)
37. D. G. Iraiyadian, S. J. Vedhagiri, M. Govindarajan and K. Parimala, Molecular dynamics simulation studies of 4-(trifluoromethyl) phenylacetonitrile, *Bulgarian Journal of Physics*, 2021, 48(4).
38. N. Gelfand, A. Freidzon and V. Vovna, Theoretical insights into UV–Vis absorption spectra of difluoroboron β-diketonates with an extended π system: An analysis based on DFT and TD-DFT calculations, *Spectrochimica Acta Part A: Molecular and Biomolecular Spectroscopy*, 2019, 216, 161–172. (https://doi.org/10.1016/j.saa.2019.02.064)
39. K. Arulaabaranam, S. Muthu, G. Mani and A. B. Geoffrey, Speculative assessment, molecular composition, PDOS, topology exploration (ELF, LOL, RDG), ligand-protein interactions, 5-bromo-3-nitropyridine-2-carbonitrile, *Heliyon*, 2021, 7(5). (https://doi.org/10.1016/j.heliyon.2021.e07061)
40. O. Kourat, A. Djafri, N. Benhalima, Y. Megrouss, N. E. H. Belkafouf, R. Rahmani et al., Synthesis, crystal structure, Hirshfeld surface analysis, spectral characterization, reduced density gradient, and nonlinear optical investigation of (E)-N'-(4-nitrobenzylidene)-2-(quinolin-8-yloxy) acetohydrazide monohydrate: A combined experimental and DFT approach, *Journal of Molecular Structure*, 2020, 1222, 128952. (https://doi.org/10.1016/j.molstruc.2020.128952)
41. K. M. Chandini, F. H. Al-Ostoot, E. E. Shehata, N. Y. Elamin, H. Ferjani, M. A. Sridhar and N. K. Lokanath, Synthesis, crystal structure, Hirshfeld surface analysis, DFT calculations, 3D energy frameworks studies of Schiff base derivative 2,2′-((1Z,1′Z)-(1,2-phenylene bis(azanylylidene)) bis(methanylylidene)) diphenol, *Journal of Molecular Structure*, 2021, 1244, 130910. (10.1016/j.molstruc.2021.130910)
42. P. Mazumdar, A. Kashyap and D. Choudhury, Investigation of hydrogen bonding in small nucleobases using DFT, AIM, NCI and NBO technique, *Computational and Theoretical Chemistry*, 2023, 1226, 114188.

(10.1016/j.comptc.2023.114188)

43. L. E. Hatcher, L. K. Saunders and B. A. Coulson, Uncovering the role of non-covalent interactions in solid-state photoswitches by non-spherical structure refinements with NoSpherA2, *Faraday Discussions*, 2023, 244, 370–390. (https://doi.org/10.1039/D2FD00158F)
44. T. Lu and Q. Chen, Visualization analysis of weak interactions in chemical systems, *Comprehensive computational chemistry*, 2024, 2, 240–264. (http://dx.doi.org/10.1016/B978-0-12-821978-2.00076-3)
45. K. Arulaabaranam, G. Mani and S. Muthu, Computational assessment of wave function (ELF, LOL) analysis, molecular confirmation, and molecular docking explored 2-(5-Amino-2-Methylanilino)-4-(3-pyridyl) pyrimidine, *Chemical Data Collections*, 2020, 29, 100525. (https://doi.org/10.1016/j.cdc.2020.100525)
46. S. Kansız, M. Azam, N. Dege, N. Ermiş, S. I. Al-Resayes and M. Alam, Supramolecular assembly in designing co-crystals of fumaric acid and pyrimidine/picolinate derivatives, *Green Chemistry Letters and Reviews*, 2022, 15(3), 825–836. (10.1080/17518253.2022.2130016)
47. J. C. Prasana, S. Muthu and C. S. Abraham, Molecular docking studies, charge transfer excitation, and wave function analyses (ESP, ELF, LOL) of valacyclovir are potential antiviral drugs, *Computational Biology and Chemistry*, 2019, 78, 9–17. (10.1016/j.compbiolchem.2018.11.014)
48. A. Demirpolat, F. Akman and A. S. Kazachenko, An experimental and theoretical study on essential oil of Aethionema sancakense: Characterization, molecular properties, and RDG analysis, *Molecules*, 2022, 27(18), 6129. (https://doi.org/10.3390/molecules27186129)
49. N. Lefi, A. S. Kazachenko, M. Raja, N. Issaoui and A. S. Kazachenko, Molecular structure, spectral analysis, molecular docking, and physicochemical studies of 3-bromo-2-hydroxypyridine monomers and dimers as bromodomain inhibitors, *Molecules*, 2023, 28(6), 2669. (https://doi.org/10.3390/molecules28062669)